Journal of Visualization, Vol. 2, No. 1 (1999) 73-84

Eulerian and Lagrangian Velocity Measurements by Means of Image Analysis

Cenedese, A.*

* University of Rome "La Sapienza," DITS, Via Eudossiana 18, 00184 - Rome, Italy.

Received 14 January 1999.

***Abstract*:** The most common velocity measurement techniques, based on image analysis (PIV), determine the velocity by correlation of a portion of the digitised images and give an Eulerian description of the investigated field. Particle Tracking Velocimetry (PTV), based on the recognition of trajectories of seeding particles, only furnishes an Eulerian description provided that the trajectories are shorter than the characteristics scale of the phenomenon. If particles are tracked for a longer time, a Lagrangian description is obtained. Consequently, in order to successfully evaluate Lagrangian statistics, a long series of single-exposed images has to be acquired. PTV has been utilised in order to analyse different laboratory simulations of flow fields which assume a particular importance in environment applications such as in the flow in a porous media and in the convective atmospheric boundary layer.

***Keywords*:** velocity, image analysis, turbulence, particle image velocimetry, atmospheric boundary layer, porous media.

1. Introduction

Velocimetry measurement techniques based on image analysis strongly depend on the level of seeding of the working fluid. This level can be defined by comparing the mean particle distance with the particle displacement between two successive acquisitions; that is with the smallest spatial scale of the velocity field structure which can be observed (Cenedese and Querzoli, 1997). If the mean distance is smaller than this scale (high seeding levels), images are analysed by means of the (auto or cross) correlation function, and this particular technique is called Particle Image Velocimetry (PIV) (Adrian, 1991; Lorenço, 1996; Keane and Adrian, 1992; Raffel and Kompenhans, 1996). If the mean distance between particles is of the same order or larger than this scale, the statistical analysis over uniform regions is not reliable. In this case, velocity is obtained from the identification of the trajectory of each particle, and this technique is called Particle Tracking Velocimetry (PTV) (Querzoli, 1996; Virant and Dracos, 1996; Nadeem and Dracos 1993).

In PIV, the investigation field is divided into small regions that are individually analysed, and one velocity value per region is obtained. This value is representative of the velocity of all the particles found on the analysed area. This means that PIV results in a succession of velocity values at fixed locations (i.e., in an Eulerian description of the velocity field).

Conversely, PTV gives velocity samples along the particle trajectories, that is in a Lagrangian frame of reference. If the length of the trajectories is small compared to the characteristic scale of the fluid motion, the information is "locally Lagrangian." It differs from that obtained from PIV only because the velocity is measured at random locations instead of over a regular grid (one sample per tracked particle is measured rather than averaging over an interrogation area). From the random distribution of samples, the velocity field over a spatial grid can be evaluated by interpolation.

Nevertheless, there are some phenomena that are naturally described in a Lagrangian frame of reference. For example, in studying pollutant dispersion, the dispersion coefficient can be computed according to the Taylor theory from particle displacements statistics (Monin and Yaglom, 1971). For the full Lagrangian description, particles have to be tracked for a period of several time scales of the phenomenon. This is possible only if a long series of single-exposed images is

acquired so that the number of particle images to be taken into account, for the trajectory recognition at each time, does not depend on the total length of the acquisition. It may be noticed that from a Lagrangian data set, both Lagrangian and Eulerian statistics can be evaluated. While the calculation of Lagrangian statistics from an Eulerian data set is much more complicated since it involves the integration in time of the instantaneous Eulerian velocity field.

2. Lagrangian Statistics

In PTV, seeding particles are followed during their motion within the measuring volume by evaluating the velocity from the displacement of each particle from one image to the next. The velocity samples are associated to fluid particle rather than merely to a location (i.e., in a Lagrangian reference frame). In general, 3-D PTV measurements are possible (Nadeem and Dracos, 1993; Virant and Dracos, 1996). Nevertheless, in the present experiment only two components of particle location and velocity are determined. This means that only the statistics involving the two measured components are evaluated.

Let T be the total acquisition time and Δt the time interval between subsequent images. The position of a particle is known at a discrete series of times $t_j=j\cdot\Delta t$, $j=1, ..., N$, where $N=T/\Delta t$. Each successful tracking of a particle gives a trajectory described by the vector (Monin and Yaglom, 1971)

$$\boldsymbol{X} = \boldsymbol{X}(m,j) \tag{1}$$

that indicates the position as a function of the particle, m, and of discrete time, j. To identify the particles, a progressive numeration is used instead of the initial position of the particle because not all particles are present at the initial time. Since the particles can leave or enter the measuring volume during the acquisition, the trajectory is known only between its initial time, jo_m, and its final time jf_m. The velocity field is expressed as a discrete function of the trajectory (1):

$$\boldsymbol{U}(m,j) = \left.\frac{\partial \boldsymbol{X}(m,t)}{\partial t}\right|_m = \frac{\boldsymbol{X}(m,j+1) - \boldsymbol{X}(m,j-1)}{2\Delta t} \tag{2}$$

In an Eulerian framework, provided that the phenomenon is steady and ergodic, the statistics can be computed from the Lagrangian data by averaging samples of all the trajectories that reach given locations. For example, the mean velocity and the variance on a spatial grid is given, respectively, by:

$$\langle u(i)\rangle = \frac{\sum_m \sum_j U(m,j) f\left[\boldsymbol{X}(m,j) - \underline{\boldsymbol{G}}\cdot i\right]}{\sum_m \sum_j f\left[\boldsymbol{X}(m,j) - \underline{\boldsymbol{G}}\cdot i\right]} \tag{3}$$

and

$$\sigma_k^2(i) = \frac{\sum_m \sum_j \left(\boldsymbol{U}_k(m,j) - \langle u_k(i)\rangle\right)^2 f\left[\boldsymbol{X}(m,j) - \underline{\boldsymbol{G}}\cdot i\right]}{\sum_m \sum_j f\left[\boldsymbol{X}(m,j) - \underline{\boldsymbol{G}}\cdot i\right]} \tag{4}$$

where:

— $\underline{\boldsymbol{G}} = \begin{pmatrix} \Delta x & 0 & 0 \\ 0 & \Delta z & 0 \\ 0 & 0 & \Delta z \end{pmatrix}$ is the spatial discretisation tensor;

— $\underline{i} = \begin{pmatrix} i_x \\ i_y \\ i_z \end{pmatrix}$ is the vector of the discrete co-ordinate on the grid,

— f is a filter function of the distance between the position of the particle and a grid node; as example f can have a rectangular or Gaussian shape with given amplitude.

Furthermore, Lagrangian statistics, such as mean velocity and auto-correlation of a steady (in an Eulerian sense) ergodic phenomenon, are obtained by averaging samples from all the trajectories reaching a given location. The mean velocity is expressed as

$$\langle \boldsymbol{U}(i,n)\rangle = \frac{\sum_m \sum_j \boldsymbol{U}(m,j+n)\cdot f\left[\boldsymbol{X}(m,j) - \underline{\underline{\boldsymbol{G}}}\cdot i\right]}{\sum_m \sum_j f\left[\boldsymbol{X}(m,j) - \underline{\underline{\boldsymbol{G}}}\cdot i\right]} \tag{5}$$

the summation is limited to the trajectories long enough for the final time to fulfil the condition

$$jf_m \geq j+n \tag{6}$$

The Eulerian steadiness implies that the summation on the right side of (5) does not depend on the initial time, nevertheless, the Lagrangian average can be time dependent.

The Lagrangian correlation can be evaluated with the following relation:

$$R_{rs}(i,n)=\frac{\sum_m\sum_j U_r(m,j)\cdot U_s(m,j+n)\cdot f\left[\boldsymbol{X}(m,j)-\underline{\underline{\boldsymbol{G}}}\cdot i\right]}{\sum_m\sum_j f\left[\boldsymbol{X}(m,j)-\underline{\underline{\boldsymbol{G}}}\cdot i\right]} \tag{7}$$

The Lagrangian correlation coefficient is obtained by normalizing $R_{rs}(i, n)$ by the velocity variance at location i:

$$r_{rs}(i,n)=\frac{R_{rs}(i,n)}{\sigma_r(i)\cdot\sigma_s(i)} \tag{8}$$

In a Lagrangian framework, the large scale characteristics of the fluid motion are described by the integral Lagrangian time scale. In a non-homogeneous turbulent flow, such as that indicated in this study, some authors state that the integral of the auto-correlation coefficient is not the Lagrangian integral time scale (Thomson, 1987). Nevertheless, the above defined scale plays a fundamental role in Lagrangian stochastic models of particle dispersion as well as in the case of strong inhomogeneities of the turbulence (Monti and Leuzzi, 1996). From a theoretical point of view, it is defined as the integral of the auto-correlation coefficient, and for a discrete time series it is

$$\tau_{L,r}(X)=\Delta t\cdot\sum_{n=0}^{\infty} r_{rr}(X,n) \tag{9}$$

As a matter of fact, confidence in the evaluation of the auto-correlation decreases strongly with the time interval n because the number of relevant trajectories decreases dramatically. Therefore, in order to represent the integral properties of the phenomenon, the $1/e$ scale $T_{L,r}$, has been chosen (Deadorf 1970; Hanna, 1981). It is defined as the time lag at which the auto-correlation coefficient is reduced to the $1/e$ value. As a consequence it is computed by taking into account only values of the auto-correlation for small, positive time lags, where the confidence is still high due to the large number of long enough trajectories.

The transport properties of the phenomenon can be investigated by a statistic that is in between the Lagrangian and Eulerian frameworks: the transilient matrix (Stull, 1993). In general, a stochastic process is completely defined by the probability density, $p(X_1, t_1, X_2, T_2)$, of particles starting at time t_1 at location X_1 and reaching location X_2 at time t_2, that is a function of 8 independent variables. If the flow field can be assumed to be steady and horizontally homogenous, the probability is only function of five independent variables. $p(z_1, z_2, t_2-t_1, x_2-x_1, y_2-y_1)$. Integrating the latter over the horizontal displacements, $\delta x=x_2-x_1$, $\delta y=y_2-y_1$, yields the probability that a particle moves from a height z_1 to another height z_2 in a given time interval $\delta t=t_2-t_1$:

$$tr(z_1,z_2,\delta t)=\int_{-\infty}^{\infty}\int_{-\infty}^{\infty} p(z_1,z_2,\delta t,\delta x,\delta y)d(\delta x)d(\delta y) \tag{10}$$

This statistic is neither Eulerian because the starting location of particles is considered, nor Lagrangian because the statistic is not computed along the trajectories. In the case of discretised height, it is a two-dimensional array function of the time lag δt, whose indexes indicate the source and destination levels.

3. Image Acquisition and Processing

In all the experiments analysed in this work the velocity is very small (less than 1 cm/s). Using a standard CCD videocamera (25 Hz frame rate), seeding particles did not move significantly from one frame to the subsequent, and the single exposure tracking technique could be used. In each experiment the thickness of the light sheet is chosen thereby taking into account the out-of-plane velocity value in order to track each particle for a time greater than the characteristic integral time scale.

The image acquisition and analysis procedure requires the following steps (Querzoli, 1996):

- The images are acquired by a CCD video-camera and recorded on tape by a video-recorder. During acquisition a frame code is inserted by an animation controller in order to identify each single frame acquired during the subsequent procedure.
- (by means of the animation controller) The frame at given time interval is automatically reached on the tape and digitised by a frame grabber on a 512 × 512 pixels × 256 grey levels array. The entire procedure is automatically controlled by a personal computer.
- The digitised frames are thresholded and centroids of the particles are computed and stored together with a time information. Only the resolution of the digitised frame, not the seeding particle dimension, affects the accuracy of measuring its positions since the the centroids of their images on the frame are considered. This accuracy is of order of the image distance that can be acquired with one pixel.
- The trajectories are recognised by looking for time-ordered centroids series that accomplish the following requirements (Fig. 1):

—The maximum distance between two particle locations must be less than a given value D (i.e., a maximum velocity assumed for the flow).

—The maximum difference between two successive displacements must be smaller than a second, given parameter e (i.e., a maximum acceleration assumed for the flow).

—A trajectory must consist of at least three particle locations.

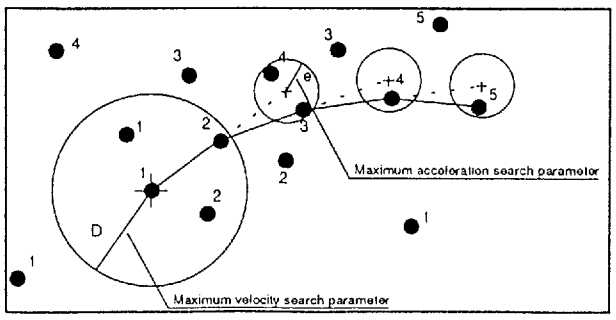

Fig. 1. Particle tracking of single-exposed images. Numbers indicate the time of acquisition of the particle cetroid locations.

The choice of the parameters D and e is crucial. if their values are too small high-speed particles are not tracked. On the other hand, if they are too large a significant number of errors occur during the trajectory reconstruction. Figure 2 shows an example of an acquired and elaborated image.

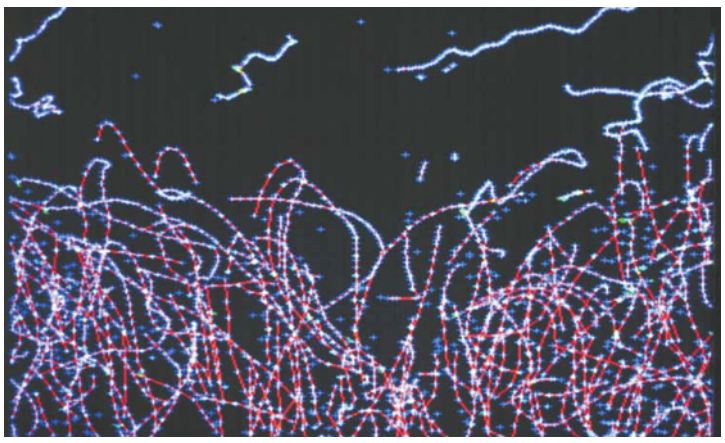

Fig. 2. A sequence of superimposed images and trajectories recognised by PTV.

4. Staturated Porous Media

In order to simulate the solid matrix of a porous medium, a rectangular tank was filled with glass cylinders containing bars of diameters d=1.0 cm broken into pieces of a length equal to 1-3 times their diameter (Cenedese and Viotti, 1996). The porosity (n) of the solid matrix obtained by randomly positioning the grains were 0.33. The bottom of a 10 cm × 10 cm × 50 cm perspex tank was connected by means of a pipe and a peristaltic pump to a vessel containing the liquid used to fill the interstices.

The vessel was filled by means of the peristaltic pump and then emptied by reversing the pump direction. During this second phase the images were acquired. To obtain optical access, the solid matrix and the liquid phase were chosen with the same refraction index (Matching Index Technique). Pyrex glass was used for the solid matrix, and fluid glycerol was found to be suitable. The high dynamic viscosity of glycerol at experimental temperature has allowed the use of micrometric air bubbles as tracers. By lighting a large portion of the test section (10 cm × 9 cm) by a 4 cm thick light sheet and filming it, it was possible to follow the trajectory of each particle for a relatively long time and so yield a Lagrangian description of the motion.

The Lagrangian approach has allowed analysis of the statistical parameters characteristic of the hydrodynamic field, such as the correlation coefficient of the velocity, the displacement covariance and the probability density function of both velocity and displacements. The acquisition carried out under the same experimental conditions (same velocity filtration) were grouped together (series).

Probability density functions (pdf) of the fluctuations of the velocity components (U'_i) were evaluated in a Lagrangian description of the motion for the images (large field) acquired under the same experimental conditions where in suitable conditions of steadiness and homogeneity were met. The high sample number (for every series the number of samples ranged between 70,000 and 200,000) together with the constraints imposed on image elaboration assured the limitation of possible error in trajectory reconstruction. The number of samples needed to achieve the steadiness of the statistics turned out to be about 20,000.

The distribution function for the longitudinal velocity fluctuation component (Fig. 3) definitely shows a non-symmetrical shape with a marked positive skewness. A chisquared goodness-of-fit test suggested that the data can be well approximated by a long normal density distribution. (Dagan, 1989). Figure 3 shows the excellent matching of experimental data with log normal distribution. It is remarkable that the absence of symmetry in the longitudinal component of the velocity is also shown by recent numerical analysis of flow in heterogenous porous formations characterized by a relatively high degree of heterogeneity for the 2D case (Bellin et. al., 1992) and for the 3D case (Levine et. al., 1992).

The pdf of the transversal velocity fluctuation component is consistently symmetrical as shown in Fig. 4 (skewness is limited to −0.53 and 0.29 for all experiments). The data do not, however, display Gaussian behaviour since the kurtosis values are between 4 and 9 for the whole series.

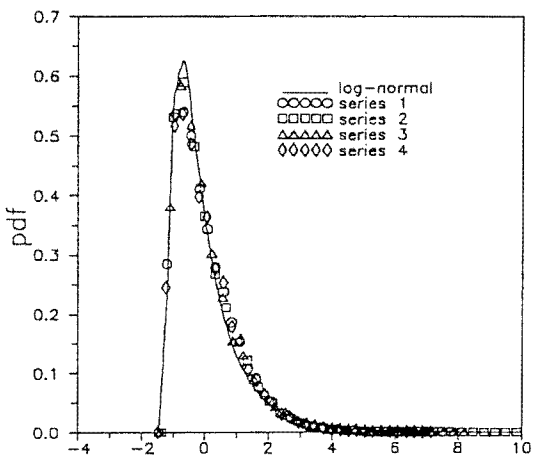

Fig. 3. Pdf of the longitudinal velocity fluctuation compoment, series 1 Re=0.032; series 2 Re=0.026; series 3 Re=0.039; series 4 Re=0.056.

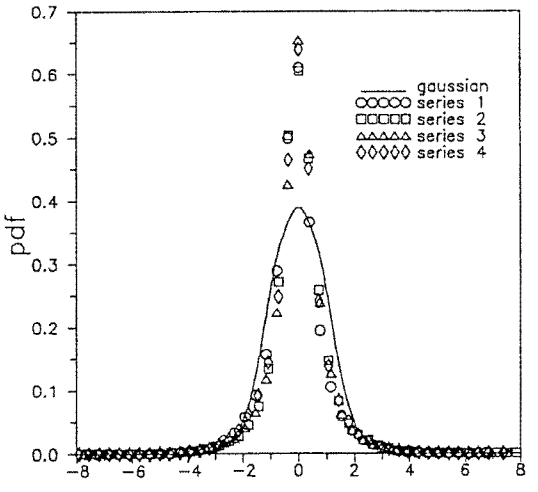

Fig. 4. Pdf of the transversal velocity fluctuation component.

Remarkable differences between the longitudinal and transversal pdfs are significant. The transversal component can be considered a random process which rapidly becomes uncorrelated and reaches a symmetrical distribution with zero skewness, which is not, however, Gaussian. The longitudinal velocity component pdf, on the other hand, has a log normal distribution as a result of local porous geometry.

The hypotheses used to analyse the dispersion process are those of statistical stationarity and homogeneity of the velocity field. Figures 5 and 6 show the autocorrelation coefficients. The evaluated cross-correlation coefficients oscillated around zero in all cases.

The high number of velocity vectors available derived from the analysis of more than 1800 images, coupled to the different experiments carried out under the same conditions, has permitted us to describe the statistical quantities of interest in terms of ensemble average.

Due to the fluctuations that were present in correspondence with higher travel times (caused by the low sample number), the Lagrangian integral scales were determined when the correlation coefficient assumed the 1/*e* value. Analysis of the results revealed, as expected, that lower values of the integral scale corresponded to higher filtration velocities. The experimental results showed that the velocity correlation held for lengths smaller than the typical grain sizes.

In the case of the velocity field homogeneity, the dispersion coefficient (D_{ij}) to be used in a diffusion equation is given by the following relation (Einstein, 1905; Taylor, 1921; Monin and Yaglom, 1971).

$$D_{ij} = \frac{1}{2}\frac{dC_{ij}(\tau)}{d\tau} \tag{11}$$

with C_{ij} the covariance of the particle displacements.

$$C_{ij} = \left\langle Y_i'(m,\tau)\cdot Y_j'(m,\tau)\right\rangle \tag{12}$$

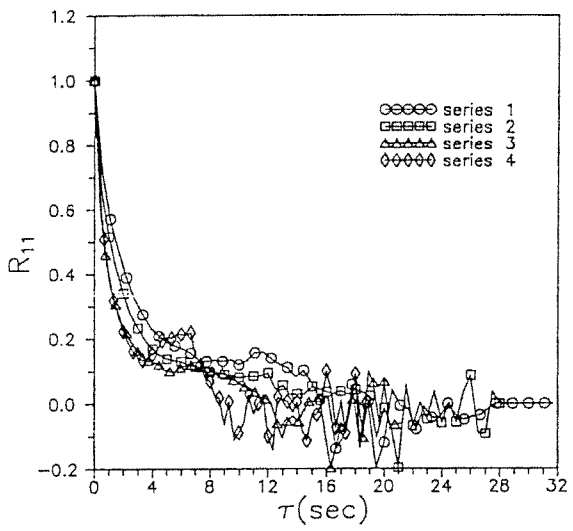

Fig. 5. Longitudinal velocity component autocorrelation coefficient.

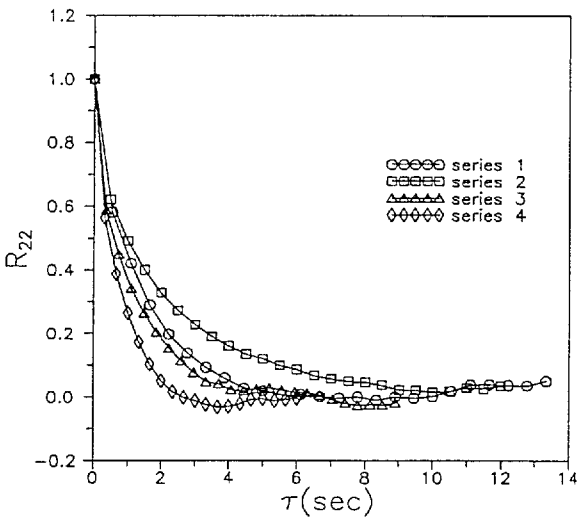

Fig. 6. Transversal velocity componet autocorrelation coefficient.

Where:

$$\boldsymbol{Y}_i'(m,\tau) = \boldsymbol{Y}(m,\tau) - \left\langle \boldsymbol{Y}(m,\tau)\right\rangle \tag{13}$$

$$\boldsymbol{Y}(m,\tau) = \boldsymbol{X}(m,\tau) - \boldsymbol{X}(m,0) = \int_{\tau} \boldsymbol{U}(m,t)dt \tag{14}$$

The relation (11) is in reality only valid if the particle displacement pdf is Gaussian or at least can be considered very similar to Gaussian (Monin and Yaglom, 1971). The obtained results for both the displacement tensor components, showed that the Gaussian pdf is reached for travel times longer than many integral scales, however, the use of the relation (11) for short travel times (if compared with the integral scales) may provide indications on plume behaviour from immission onwards. Figures 7 and 8 report the trend of the evaluated hydrodynamic dispersion components for different velocity filtration. The figures show the agreement with theories concerning the behaviour of dispersion coefficient over travel time (Monin and Yaglom, 1971; Dagan, 1989). In fact, the components start from null value and increase with time to an asymptotic value which is independent of time. Analysis of the asymptotic values shows clearly that there is an anisotropy in agreement with most of the experimental data and the theoretical models (Dagan, 1989).

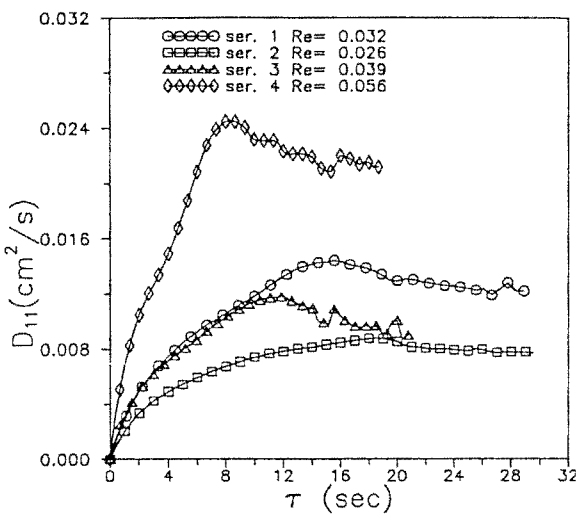

Fig. 7. Longitudinal component of the dispersion coefficient.

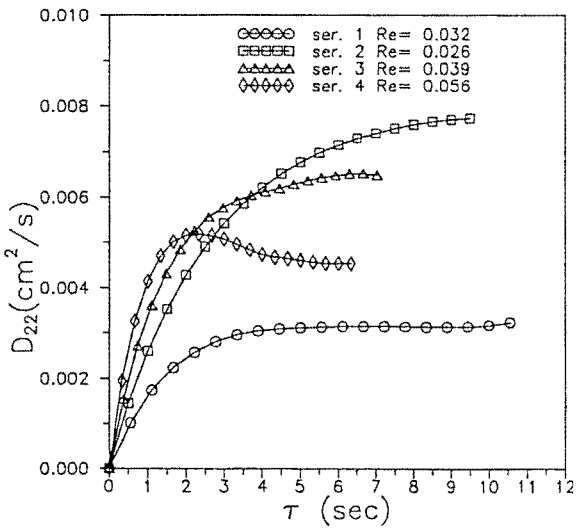

Fig. 8. Transversal component of the dispersion coefficient.

The constancy in time of the values of the components seems to be reached in faster time for the transversal component and after longer times for the longitudinal component. The asymptotic value of the longitudinal dispersion coefficient can be related directly to the average filtration velocity and to a length characteristic of the medium generally chosen as the grain length (Hulin and Salin, 1987; Charlaix et al., 1987). The experimental results suggest that the Lagrangian integral scale can be suitably chosen as a such "characteristic length."

5. Atmospheric Convective Boundary Layer

The atmospheric convective boundary layer generated by solar radiation on the soil in the late morning and early afternoon of a sunny day (above a flat terrain) was simulated by a convection chamber filled with water. The mean wind was assumed absent or very light, so that the mechanical production of turbulent kinetic energy is small compared to the buoyant production. Under these conditions, the heating of the soil generates a convective layer that is bounded from above by a thermally stable layer, namely the capping inversion, that is slowly eroded by entrainment into the lower turbulent layer.

The following steps are performed during each experiment (Fig. 9):

- The tank is filled up to 10 cm with ambient temperature water;
- A second layer, 10 cm high, of hot water (20 ; higher than ambient temperature) is stratified above the first one to generate a thermally stable zone that simulates the Capping Inversion of the atmosphere;
- After about 5 minutes that the heating at the lower surface has been applied (simulating the solar heating of the soil), the turbulent convection is completely developed and acquisition starts.

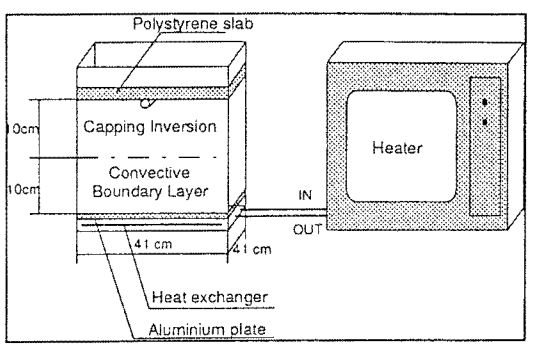

Fig. 9. Sketch of the convection chamber and heating system.

The comparison with atmospheric phenomena and convection occurring in the water tank is possible by using the similarity proposed by Deardorff (1970). It is assumed that the scaling parameters are the convective velocity,

$w^* = \sqrt[3]{g\alpha q_s z_i}$, the height of the convective layer z_i and the convective time $t^* = z_i / w^*$ where g indicates the acceleration of gravity, α the thermal expansion coefficient, and q_s the kinematic heat flux at the surface. The results that were presented in non-dimensional form throughout this scaling are not dependent on the particular conditions of the experiment. As a consequence, the non-dimensional Eulerian statistics do not vary with time provided that convection is fully developed. It was observed that, 5 mins after the heating has been applied, the vertical profiles of Eulerian non-dimensional statistics obtained from the data sampled during the different time intervals do not vary anymore (Cenedese and Querzoli, 1994). As a consequence the phenomenon was considered quasi-steady after that time.

Due to the dimension of the measuring volume and to errors during the tracking, the number of recognised trajectories decreases rapidly in their length. This is shown in Fig. 10 where the probability density of trajectory length is presented as a function of the non-dimensional time.

In an Eulerian frame of reference, the phenomenon is steady and the probability density distribution of the vertical velocity is not symmetrical, with a slightly negative mode (Fig. 11). Because the convective boundary layer is characterised by small and intense updrafts and large but slow downdrafts (Deardorff and Willis, 1985; Stull, 1988; Hunt et al, 1988).

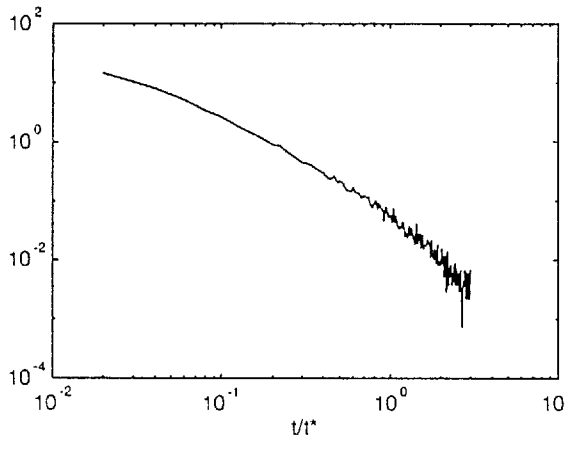

Fig. 10. Probability density distribution of trajectory length as a function of the non-dimensional time.

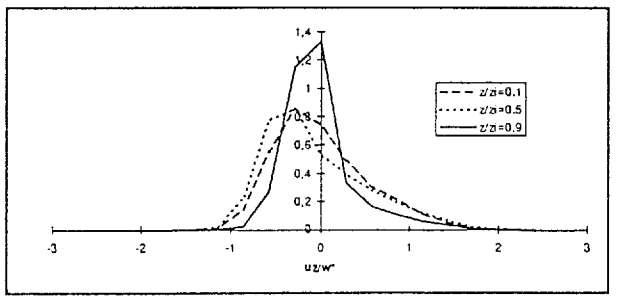

Fig. 11. Probability density distribution of the non-dimensional vertical velocity.

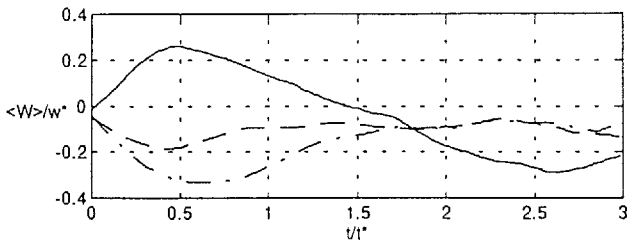

Fig. 12. Mean vertical velocity as a function of time in the Lagrangian reference frame at z/z_i=0.25 (solid line), z/z_i=0.55 (dashed line), z/z_i=0.75 (point-dashed line).

The Lagrangian mean vertical velocity, at three different level, is presented in Fig. 12 as a function of the non-dimensional time.

Although the phenomenon is steady from the Eulerian point of view, this is not the case in a Lagrangian framework. The mean velocity varies with time because this statistic is evaluated along the trajectories of particles that move around within the layer and different conditions. Only the asymptotic limit is zero, that is as far as the velocities are completely uncorrelated. The mean velocity of particles starting close to the ground increases for short times because they cross layers with higher velocity, and an opposite trend is observed for the particles starting close to the capping inversion.

The non-symmetry of the Lagrangian auto-correlation coefficient, plotted in Fig. 13 at three different heights, confirms the Lagrangian non-steadiness of the phenomenon. Since the normalisation of the correlation coefficients is done by means of the Eulerian variance at the starting level of the trajectories, they are not defined less than one as in the case of classical Eulerian coefficients; nevertheless, in this way the original shape of the function is preserved.

The different behaviour of the hot updrafts and cold downdrafts has been pointed out by the conditional sampling. The ensemble of trajectories has been divided into two sets: the first one includes trajectories that initially move upwards, and the second one includes trajectories that initially move downwards. Statistics have been computed separately for the two sets (Fig. 14).

The correlation coefficient of the vertical velocity is not maximum for a zero time lag: particles rising from the lower part of the layer (z/z_i=0.25) exhibit a maximum correlation for a slightly positive time lag since they are slow in the proximity of the surface and accelerate through the whole depth of the layer. On the contrary, descending particles found in that region decelerate as they get closer to the lower surface and exhibit the maximum correlation at a negative time lat. This behaviour is not apparent at mid-height (z/z_i=0.55) where no sudden changes in particle velocity are imposed by close boundaries. In the upper part of the layer (z/z_i=0.75) symmetrical behaviour is observed. Due to the presence of the capping inversion, ascending particles decelerate, and their correlation is a maximum for slightly negative time lags. Descending particles, however, accelerate and exhibit the maximum correlation for a positive time lag.

According to this behaviour, the 1/*e* Lagrangian time scale, T_L, of the vertical velocity, computed for positive time lags (Fig. 15), increases with height for the updrafts since this scale is related to the time taken by the particles to reach the capping inversion.

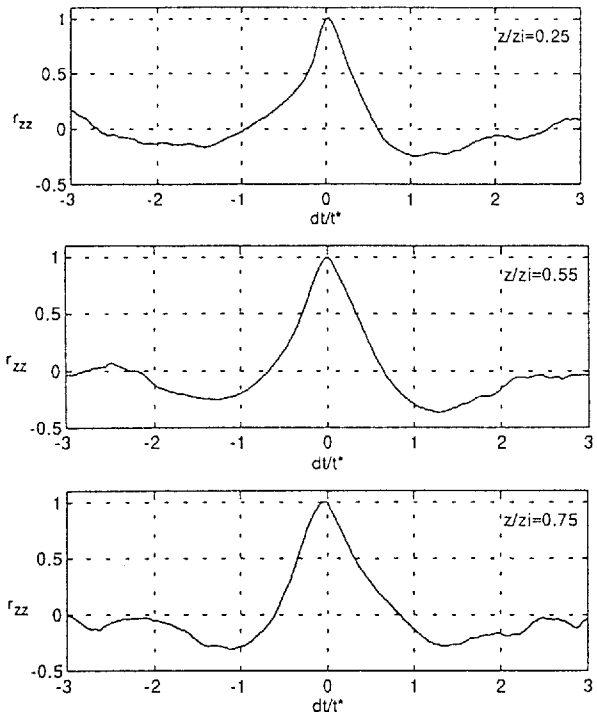

Fig. 13. Lagrangian auto-correlation coefficient of the vertical velocity at three different heights.

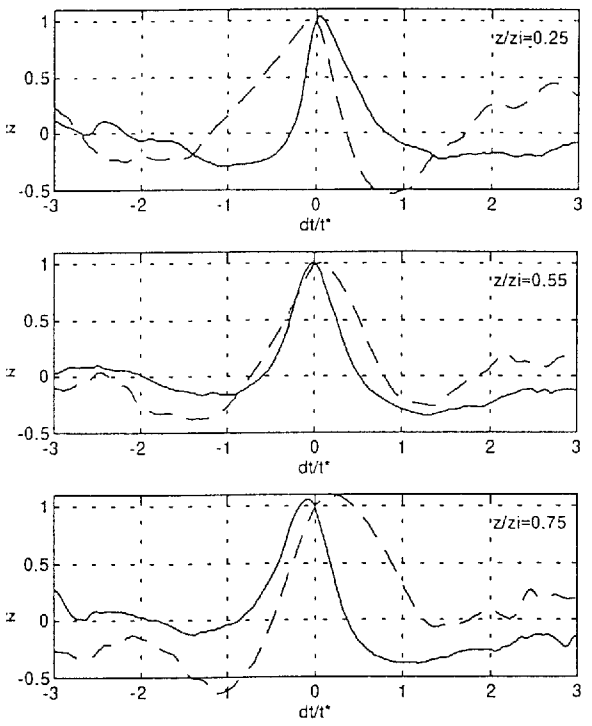

Fig. 14. Lagrangian auto-correlation coefficient of the vertical velocity at three heights. Dashed lines indicate the downdrafts, solid line updrafts.

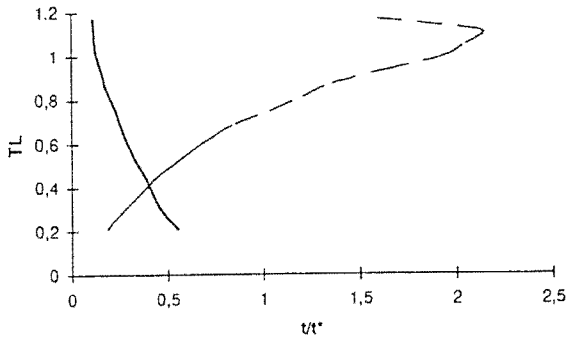

Fig. 15. 1/*e* time scale of the updrafts (solid line) and downdrafts (dashed line) as a function of the non-dimensional height.

However the behaviour of the descending particle 1/*e* time scale is different since, in this case, the scale is related to the time that particles take to reach the lower surface. The downdraft time scales are generally larger than the updraft ones because they are characterised by lower velocity, according to the probability density distribution shown in Fig. 11.

A more detailed description of the mixing process can be obtained from the analysis of the transilient matrix. Assuming horizontal homogeneity, and dividing the investigation field into layers, this matrix represents the fraction of fluid advected from one layer to another in a given time interval. Its first index shows the destination level of mixing and the second the source level. In Fig. 16 the transilient matrix is presented for four time intervals; the rows of the matrix are plotted in reverse order to have the height axis increasing upwards. The elements of the main diagonal indicate the fraction of fluid that does change layer in the given time. For small time intervals mixing is concentrated close to this zone since particles have not time to mix. As time increases, larger and larger zones of the matrix are affected by mixing and have non-zero values. For times larger than t_* all the convective layer is mixed ($z/z_i<1$) whereas the high values of sources and destinations larger than z_i remain concentrated close to the main diagonal, giving the evidence that the capping inversion does not participate in the mixing phenomena and pollutants are confined in the convective layer.

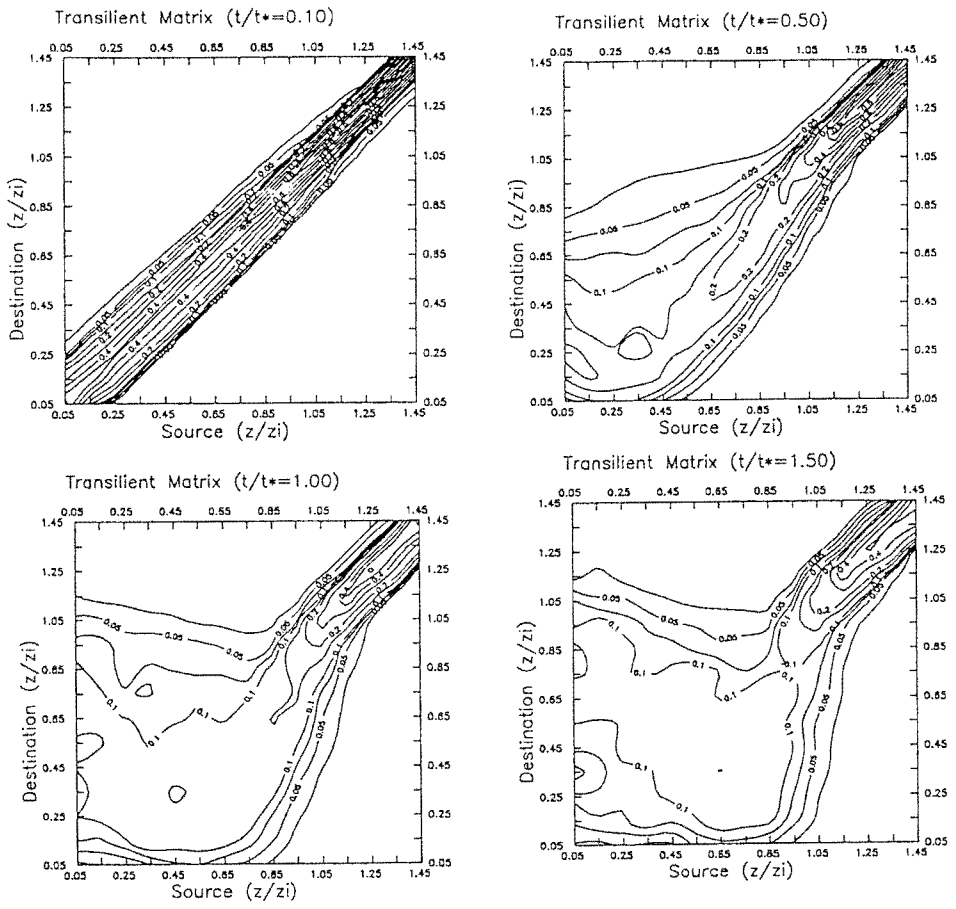

Fig. 16. Transilient matrix at different time intervals.

References

Adrian, R. J., Particle-image Techniques for Experimental Fluid Mechanics, Ann. Rev. Fluid Mech., 23, (1991), 261-304

Bellin, A., Salandin, P. and Rinaldo, A., Simulation of Dispersion in Heterogeneous Porous Formations: Statistics, First-Order Theories, Convergence of Computations, Water Resourc. Res., 28(9), (1992), 2221-2227

Cenedese, A. and Querzoli, G., A Laboratory Model of Turbulent Convection in the Atmospheric Boundary Layer, Atmos. Env., 28, (1994), 1901-1904

Cenedese, A. and Querzoli, G., Lagrangian Statistics and Transilient Matrix Measurements by PTV in a Convective Boundary Layer, Meas. Sci Technol., 8, (1997), 1553-1561

Cenedese, A. and Viotti, P., Lagrangian Analysis of Nonreactive Pollutant Dispersion in Porous Media by Means of the Particle Image Velocimetry Technique, Water Resources Research, 32(8), (1996), pp. 2329-2343

Charlaix, E., Hulin, J. P., and Plona, T. J., Experimental Study of Tracer Dispersion in Sintered Glass Materials of Variable Compaction, Physics of Fluids, 30 (6), (1987), 1690-1698

Dagan, G., Flow and Transport in Porous Formations, Springer-Verlag (1989)

Deardorff, J. W., Convective Velocity and Temperature Scales for the Unstable Planetary Boudary Layer and for Rayleigh Convection, J. Atmos. Sci., 27, (1970), 1211-1213

Deardorff, J. W. and Willis, G. E., Further Results from a Laboratory Model of the Convective Planetary Boundary Layer, Boundary-Layer Met.,

32, (1985), 205-236
Einstein, A., On the Movement of Suspended Particles in Stationary Fluids Deduced from Molecular-Kinetic Theory of Heat (in German), Ann. Phys., 17, (1905), 539-560
Hanna, R. S., Lagrangian and Eulerian Time-scale Relations in the Daytime Boundary Layer, J. Appl. Meteorol., 20, (1981), 242-249
Hullin, J. P, and Salin, D., Experimental Study of Tracer Dispersion in Model and Natural Porous Media, Disorder and Mixing Convection, Diffusion and Reaction in Random Materials and Processes, Nato ASI Series: Series E, Vol. 152. (1988)
Hunt, C. R., Kaimal, J. C. and Gaynor, J. E., Eddy Structure in the Convective Boundary Layer - New Measurements and New Conepts, Q.J.R. Met. Soc., 114, (1988), 827-870
Keane, R. D. and Adrian, R. J., Theory of Cross-correlation Analysis of PIV Images, Appl. Sci.Rev., 19, (1992), 191-215
Levine, O., Zhang, D. and Neumann, S. P., Statistical Properties of Steady-state 3d Eulerian and Lagrangian Velocity Fields, Fall Meeting American Geophisical Union Published Ass. to EOS, (1992).
Lorenço, L. M., Hisorical Background, Mathematical Tools in PIV, Processing Techniques, Lecture Series, v. Karman Institute of Fluid Dynamics
Monin, A.S. and Yaglom, A.M., Statistical Fluid Mechanics, MIT Press, (1971), Cambridge
Monti, P., Leuzzi, G., A Clusure to Derive a Three-dimensional Well-mixed Trajectory Model for Non-Gaussian, Inhomogeneous Turbulence, Boundary-Layer Met., 80, (1996), 311-331
Nadeem, A. M. and Dracos, Th., Lagrangian PTV in 3D Flows, Appl. Sci. Res., 51, (1993), 161-166
Querzoli, G., A Lagrangian Study of Particle Dispersion in the Unstable Boundary Layer, Atmos. Env., 30, (1996), 2821-2829
Raffel, M. and Kompenhans, J., Theoretical and Experimental Aspects of PIV Recording Utilizing Photographic Film and Mechanical Image Shifting, Lecture Series, v. Karman Institute of Fluid Dynamics (1996)
Stull, R. B., An Introduction to Boundary Layer Meteorology, Kluwer Academic Publishers, Dordrecht (1988)
Stull, R. B., Review of Transilent Turbulence Theory and Nonlocal Mixing, Boundary -Layer Meteorol., 62, (1993), 21-96
Taylor, G. I., Conditions under which Dispersion of a Solute can be Used to Measure Molecular Diffusion, Proc. R. Soc. London A, 225, (1954), 473-477
Thomson, D. J., Criteria for Selection of Stochastic Models of Particle Trajectories in Turbulent Flows, J. Fluid Mech., 180, (1987), 529-556
Virant, M. and Dracos, Th., An Application of 3D-PTV on the Measurement of Turbulent Quantities and Particle Dispersion in Turbulent Channel Flow, in Advances in turbulence VI, S. Gavrilakis et al. (eds), Kluwer Academic Publishers, The Netherlands (1996), 499-502
Willis, G. E. and Deardorff, J. W., A Laboratory Model of the Unstable Planetary Boundary Layer, J. Atmos Sci., 31, (1974), 1297-1307

Author's Profile

Antonio Cenedese: He received the degree in Mechanical Engineering in 1966 and the degree in Aerospace Engineering in 1969 from the University of Rome "La Sapienza."
Researcher starting from 1969, Associate Professor from 1976 and Professor from 1986.
His research field is fluid mechanics, mainly experimental analysis in turbulent flows by means of laser Doppler anemometry and particle image velocimetry. Recently particular attention has been devoted to environmental fluid dynamics.